



Shuai Yuan and Deren Yang

Contents

Introduction	464
Basic Properties of Nitrogen in Silicon	465
Existence	465
Detection and Measurements	466
Solubility	468
Diffusion	469
Nitrogen in Czochralski Silicon	470
Doping of N in CZ-Si Growth	470
N-O Complexes	471
Influence on O-Related Defects	474
Effect of N Impurity on Mechanical Properties	476
Nitrogen in Cast Multicrystalline Silicon	478
Soluble Nitrogen	478
Silicon Nitride Precipitates	482
Influence on Wafering and the Mechanical Strength of Wafers	483
Influence on Electric Properties of Cell Performance	485
Growth of Multicrystalline Silicon in Ambient Nitrogen	485
Gas Doping of N for Cast Mc-Si	485
Improvement in Mechanical Strength	487
Impact of N-O Complexes in Mc-Si Grown in Ambient N ₂	488
Conclusion	490
Cross-References	490
References	490

S. Yuan (✉)

State Key Laboratory of Silicon Materials and school of Materials Science and Engineering,
Zhejiang University, Zhejiang, Hangzhou, China
e-mail: shuaiyuan@zju.edu.cn

D. Yang

State Key Laboratory of Silicon Materials and school of Materials Science and Engineering,
Zhejiang University, Hangzhou, China
e-mail: mseyang@zju.edu.cn

Abstract

This chapter starts with the basic features of nitrogen including the existence of N-related defects, detection and measurements of N content, the solubility, and diffusion of N impurities in silicon materials. From the perspective of photovoltaic application, the nitrogen doping method for Czochralski silicon is then introduced, and the results about the influence of nitrogen impurity on N-O complexes, O-related defects, and mechanical properties are presented. A second focus of this chapter is toward N-related defects in directionally solidified photovoltaic multicrystalline silicon (mc-Si) materials. The existence and distribution of N-related defects, the formation, and influence of silicon nitride precipitates in mc-Si are comprehensively described. Then the results about mc-Si growth in ambient nitrogen are presented as an application to further understand the properties of nitrogen in mc-Si.

Keywords

Czochralski silicon · Multicrystalline silicon · Nitrogen doping · Silicon nitride precipitates · Ambient nitrogen · Mechanical strength

Introduction

Crystalline silicon (c-Si) is the most important substrate material for solar cells, which occupies more than 90% of the market share in photovoltaic industry. Czochralski silicon (CZ-Si) and cast multicrystalline silicon (mc-Si) are the main types of c-Si materials. Nitrogen is one of the common light elemental impurities in silicon materials. Related research started decades ago. In the 1970s, nitrogen property in nitrogen-implanted silicon, Si_3N_4 films on silicon substrate and even in float-zone silicon was widely studied. And in the 1980s, nitrogen was intentionally doped in CZ-Si wafers used for integrated circuit (IC) industry (Que et al. 1985; Yang et al. 1995). Due to the suppression of crystal-originated particles (COPs) (Yu et al. 2002), the enhancement on the nucleation of oxygen precipitates so as to improve the ability of internal gettering, and the increasement of mechanical strength, N-doped CZ-Si has been world widely applied (Yang et al. 2009; Yu et al. 2013). Moreover, N-doping in CZ-Si can also reduce high purity argon gas consuming expense, which helps to decrease the general cost of silicon crystal growth.

However, for photovoltaic materials as substrates of bulk devices, the modification by introducing oxygen precipitates is unwanted. Then the promising feature of nitrogen doping in CZ-Si crystal is to improve the material mechanical strength and to reduce the cost of protective gas by using cheaper nitrogen instead of high purity argon. So, intentional N-doping in CZ-Si becomes less attractive to photovoltaic manufactures. In the recent two decades, directionally solidified mc-Si has gradually become the leading photovoltaic substrate materials because of its low cost. Despite nitrogen was never intended to be doped into mc-Si, silicon nitride has been the optimal coating material to prevent the sticking between silicon ingots and quartz crucibles. The usage of silicon nitride coating made mc-Si growth in a N-rich environment so that the influence of N-related defects, especially Si_3N_4 precipitates, is very important to the crystal quality.

Meanwhile, there are a few researches considering the further control of N impurity in mc-Si by other means.

This chapter firstly summarizes the basic properties of N-related impurity in general silicon materials. Then from the photovoltaic silicon perspective, we briefly introduce the influence of N-doping on the relevant properties in Czochralski silicon. Later, the existence and transformation of N-related impurity and precipitates in mc-Si are described. And finally, the growth of photovoltaic mc-Si using cheaper ambient nitrogen is presented and discussed.

Basic Properties of Nitrogen in Silicon

Existence

In crystalline silicon materials, soluble nitrogen atoms exist in the forms of monomer, dimer, or complex in Si lattice, and precipitates are formed when N concentration exceeds the solubility. Various N-containing defects can be formed based on the reaction and combination of N atoms (interstitial and substitutional, N_i , and N_s), defective Si atoms (interstitials and vacancies, I and V), and other impurity atoms like oxygen. The structure of the configurations determines the formation energy, thermal stability, and particular local vibrational modes (LVMS) of the defects. The actual form of N-related defects in a certain sample is strongly influenced by thermal history. And LVMS of the defects result in well-defined shifts in the vibrational frequencies, which help to identify the defects experimentally. The properties such as formation energy and LVMS of the N-containing configurations can be determined using first principle density functional theory; hence, the equilibrium stability can be predicted and the frequencies of the modes can be identified combined with infrared (and Raman) measurements (Jones et al. 1994b; Goss et al. 2003) (see the section “Detection and Measurements”). Table 1 gives the calculated formation energy per N atom of various combinations of N_i , N_s , I , and V , relative to the energy of the (N_i-N_i) defined as zero. The data shows that all configurations have higher formation energy compared with (N_i-N_i) , the only exception, $2(N_i-N_i)$, possesses a very small binding energy, so it should not be stable and significant. Since (N_i-N_i) has a large binding energy of 4.30 eV (Sawada and Kawakami 2000), and isolated N_i has a high mobility (see the section “Diffusion”), therefore, di-interstitial pairs (N_i-N_i) should be the dominant equilibrium state of nitrogen atoms in silicon lattice under growth temperature (>1400 °C). The vibrational frequencies of many modes

Table 1 Relative formation energies (eV) per N atom for various N configurations, zero is defined by that of (N_i-N_i) (Goss et al. 2003)

Structure	$2(N_i-N_i)$	(N_i-N_i)	(N_s-N_s)	(N_i-N_s)	$(N_i)_2I$
E_f/N atom	-0.06	0.00	0.79	0.99	1.25
Structure	$(N_s-N_s)V$	N_i	N_s	$(N_s-N_s)V_2$	(N_sV)
E_f/N atom	1.71	1.83	1.99	2.54	3.71

Table 2 Calculated and observed frequencies (cm^{-1}) of IR active local modes of ^{14}N in Si (Goss et al. 2003)

	(N_i-N_j)	N_s
Calculated	967.8/772.9	637
Observed	962.1/765.6	653

have been investigated (Goss et al. 2003), among which, Table 2 shows the calculated and observed frequencies of the vibration modes of $(^{14}\text{N}_i-^{14}\text{N}_j)$ and $^{14}\text{N}_s$. These two modes are the only detectable modes at room temperature verified in experimental measurements (Goss et al. 2003). Moreover, the fraction of N_s in total N atoms is lower than 1%, which indicates that the final state of N dimer at room temperature is (N_i-N_j) and the concentration of N_s in normal N-doped Si is usually lower than 10^{13} cm^{-3} . Therefore, the influence of ionized N_s donors on electrical properties can be ignored.

Detection and Measurements

To date, secondary ion mass spectroscopy (SIMS) and Fourier transformation infrared spectroscopy (FTIR) are the most widely used methods to determine the N concentration in crystalline silicon. SIMS is usually adopted for total N concentration, independent of its chemical states, the lower detection limit can be extended to $1 \times 10^{13} \text{ cm}^{-3}$, but the measurement is relatively complicated and expensive when the N concentration is lower than $5 \times 10^{14} \text{ cm}^{-3}$, mainly limited by the background N concentration (Hockett and Sams 2000). IR measurements via the presence of N-related vibration modes can differentiate the forms of N atoms in silicon, as these modes have different absorption frequencies. Figure 1 shows the example of a mid-infrared range FTIR spectrum at room temperature. The quantitative measurement of concentration can be obtained from the absorbance at certain peaks:

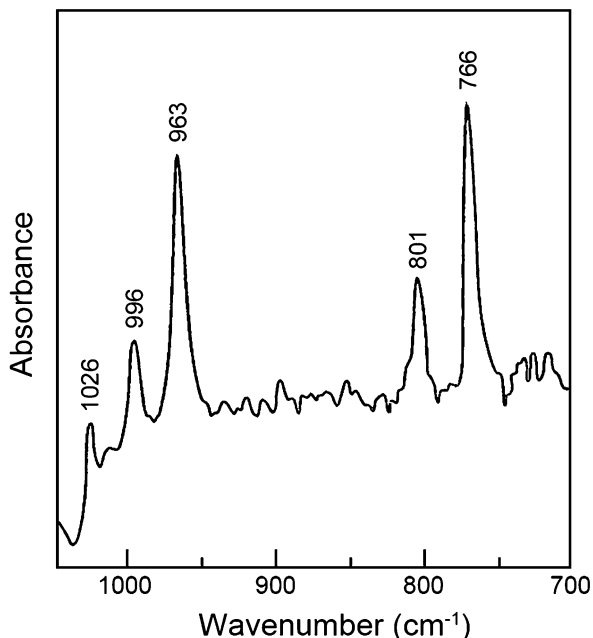
$$C = \frac{1}{d} \alpha A = \frac{1}{d} \alpha \ln \left(\frac{I_0}{I} \right),$$

where C is the impurity concentration, d is the sample thickness, α is the absorption coefficient, A is the absorbance at the peak, and I_0 and I are the IR signal intensity of the peak and baseline, respectively.

N dimers exhibit main IR vibration absorption peaks at 963 and 766 cm^{-1} , with the calibrated absorption coefficients of 1.83×10^{17} (Itoh et al. 1985) and $4.45 \times 10^{17} \text{ cm}^{-2}$ (Wagner et al. 1988), respectively. This method ensures a detection limit of $\sim 5 \times 10^{14}/d \text{ cm}^{-3}$ ($\sim 100/d$ ppba, the unit of d is cm).

As the main form of N in Si under room temperature is N dimer and N-O complex, in oxygen-free float-zone silicon (FZ-Si), the total N concentration measured by SIMS equals to the N concentration measured by FTIR (963 cm^{-1}), which

Fig. 1 FTIR absorption peaks of N dimer ($766, 963\text{ cm}^{-1}$) and N-O ($801, 996, \text{ and } 1026\text{ cm}^{-1}$) complex at room temperature



proves that the main existing form of N in FZ-Si is N dimers. However, in CZ-Si and mc-Si, the N dimer concentration measured by FTIR is lower than the one measured by SIMS, due to the formation of N-O complexes and the decrease in N dimer concentration. As shown in Fig. 1, N-O complexes also exhibit a series of IR vibration absorption peaks (including $801, 996, \text{ and } 1026\text{ cm}^{-1}$) (Qi et al. 1991), without well-accepted absorption coefficient. The isotopic effects on these LVMs show that these modes all shift with ^{15}N (Jones et al. 1994a), showing N atoms to be involved in the complexes. Especially, the absorption intensity of 801 cm^{-1} has a linear dependence on the product of $[\text{N}][\text{O}_i]$, indicating that these bands arise from the N-O complexes. Therefore, FTIR at room temperature cannot be used to estimate the total N concentration in CZ-Si. While it is controversial to measure total N content in mc-Si because the interstitial oxygen concentration in mc-Si varies with growth details, so that a coarse measurement of total N content using N dimer IR absorption is somehow acceptable.

Low-temperature Fourier transformation infrared spectroscopy (LT-FTIR) helps to extend the detection limit. On one hand, the 963 cm^{-1} IR peak of N dimers shifts to 967 cm^{-1} and becomes narrower when the sample is cooled down to 77 K, with a calibrated absorption coefficient of $1.2 \times 10^{17}\text{ cm}^{-2}$ (Zhang et al. 2013), lower than the one under room temperature, which extends the N dimer detection limit to $\sim 2 \times 10^{14}\text{ cm}^{-3}$ at 77 K. On the other hand, the determination of N concentration in CZ-Si lower than 10^{14} cm^{-3} can be performed using LT-FTIR in far-infrared range. The absorption peaks correspond to the ionization levels of the N-O complex

donors in silicon, in the spectral range of 190–350 cm^{-1} . (see the section “N-O Complex” part) Before the measurement, long-time thermal annealing (mostly at 500–650 $^{\circ}\text{C}$) is needed to assure saturated transformation from N dimers into N-O complexes. The detection limit of LT-FTIR method is affected by signal intensity of the spectrometer and sample thickness. Several detection limits have been reported in the range of $5\text{--}90 \times 10^{12} \text{ cm}^{-3}$ (Nakatsu et al. 2004; Ono and Horikawa 2003; Porrini et al. 2003). Nevertheless, the calibration of IR absorption into absolute concentration is not enough by now.

In addition, there are many other detection techniques for N-related contents in Si, including charged particle activation analysis (CPAA) (Nozaki et al. 1970), deep level transient spectroscopy (DLTS) (Tokumaru et al. 1982), Rutherford backscattering spectrometry (RBS), Auger electron spectroscopy (AES), electron paramagnetic resonance (EPR), luminescence and electrical resistivity (Bucksbaum and Bokor 1984; Hemment et al. 1985). Some of these methods were used to measure implanted substitutional N atoms in the early researches. However, most of them could not reach the sensitivities required to measure a common concentration of N in photovoltaic CZ-Si and mc-Si as low as 10^{15} cm^{-3} .

Solubility

The nitrogen solubility in molten silicon was measured as $6 \times 10^{18} \text{ cm}^{-3}$ by charged particle activation analysis (CPAA), using a sample at the end of fast cooled FZ-Si ingot (Yatsurugi et al. 1973). When N concentration in molten silicon exceeds the solubility, $\beta\text{-Si}_3\text{N}_4$ rods/particles will be segregated and float above the molten silicon. This phenomenon can be commonly observed in the growth industrial directionally solidified mc-Si ingots because the soluble N is usually saturated in the molten silicon at the end of growth, however, floating Si_3N_4 in CZ growth may cause failure of dislocation-free growth.

The solid solubility of N in Si was initially measured and reported as $(4.5 \pm 1) \times 10^{15} \text{ cm}^{-3}$ (Yatsurugi et al. 1973), which was determined by the solubility in molten silicon and the small equilibrium segregation coefficient of N in Si ($k_0 = 7.5 \times 10^{-4}$ (Yatsurugi et al. 1973)). However, a larger solid N concentration at room temperature was measured as $\sim 1 \times 10^{16} \text{ cm}^{-3}$ (FTIR, 963 cm^{-1}) in directionally solidified mc-Si, where the effective segregation coefficient of N, k_{eff} , became larger than k_0 due to the moderate convective transportation in casting method. According to Burton-Prim-Slichter theory, k_{eff} is defined by the following formula:

$$k_{\text{eff}} = \frac{k_0}{k_0 + (1 - k_0)\exp(-R\delta_{\text{BPS}}/D_L)}$$

where R is the growth rate and δ the thickness of boundary layer which is determined by diffusivity (D_L) of N and convection level. Obviously, compared to CZ growth, casting growth has much weaker convection level so that the boundary layer is

thicker and then the k_{eff} become larger. As the N concentration in solidified mc-Si is determined by both the N concentration in molten silicon and segregation effect, which are all strongly affected by convection level, N concentration in molten silicon is also influenced by crucible size and diffusion time, which may cause very complicated local distribution in the whole system. In the cases with weak convection, the N concentration at ingot center is lower than that at the edge, but as the segregated N in the molten silicon increases fast, the N concentration in solid phase can keep increasing along ingot height due to segregation effect. Once the concentration (FTIR, 963 cm^{-1}) in solid phase exceeds 10^{16} cm^{-3} , Si_3N_4 precipitates will be rapidly generated, along with the decrease in N dimer IR absorption (Reimann et al. 2010) because the N dimers will further segregate on the precipitates. Therefore, the solid solubility of N in Si is usually noted as $(4\text{--}10) \times 10^{15} \text{ cm}^{-3}$.

Diffusion

The diffusivity of N in silicon is controversial during the past decades because of the many forms of N-related defects. Researchers have reported theoretical and experimental results of various diffusion models. Theoretical investigation results indicate that the N monomer has a migration activation energy of 0.4 eV (Schultz and Nelson 2001; Nelson et al. 1998), which means they are highly mobile under high temperature. But the experimental measurements of the N monomer diffusivity in silicon are limited to its relatively low concentration and the detective techniques. Table 3 gives several experimental results, where the diffusion coefficient is expressed by Arrhenius formula:

$$D = D_0 \exp\left(-\frac{E_A}{kT}\right)$$

where D is the diffusion coefficient (cm^2/s), D_0 is the pre-exponential factor (cm^2/s), E_A is the migration activation energy (eV), T is the absolute temperature (K), and k is the Boltzmann constant, $1.38064 \times 10^{-23} \text{ m}^2 \cdot \text{kg} / \text{s}^2 \cdot \text{K}$.

The first measurement of N diffusion coefficient attempted by Clark et al. was based on Hall effect (Clark et al. 1968). After implanting $^{14}\text{N}^+$ ions to form an n -type

Table 3 The pre-exponential factor (D_0) and migration activation energy (E_A) of various models of N in silicon

	D_0 (cm^2/s)	E_A (eV)	Model
Clark et al. (1968), Pavlov et al. (1976)	0.87	3.29	Ion-implanted N
Itoh and Abe (1988)	2.7×10^3	2.8	N dimer
Voronkov and Falster (2004)	0.25	1.25	N monomer from the dissociation of N dimer
Murphy et al. (2005)	6.3×10^{-2}	1.38	Pinning of N monomer at dislocations

surface layer in the high resistive *p*-type silicon, the evolution of the *p-n* junction depth with the anneal temperature and time reflects the $^{14}\text{N}^+$ diffusion behavior. Obviously, this experiment is not reliable for the major form of N dimers in N-doped CZ-Si and mc-Si.

The most well-accepted diffusivity of N dimers was based on N dimer model. Theoretical results show that dominant N dimers have a large migration activation energy of 2.5 eV (Sawada et al. 2002; Fujita et al. 2005; Stoddard et al. 2005), which is assumed to be practically immobile at room temperature, indicating the diffusion of N dimers happens before a sample is cooled. Itoh et al. used SIMS (Itoh and Abe 1988) to measure out-diffused N on the profiles of silicon. It was found that the total amount of out-diffused N corresponds with the variation of N dimer IR absorption at the frequency of 963 cm^{-1} , confirming that the N impurities in silicon diffuse as the form of dimers. The experimental value of activation energy was measured as 2.8 eV, which is close to the calculated values using first principle method, so this model is supported by theoretical investigations.

Moreover, further experiments suggest that the diffusivity of N in silicon is more complicated when the influence of other parameters such as oxygen impurities or dislocations is considered. Hockett (1989) suggested that N dimers may not be the only species responsible for transport, since a small fraction of N diffused rapidly while the majority (N dimers) remained immobile. Later, Mannino et al. found that N diffusion can be enhanced in oxygen-rich CZ-Si (Mannino et al. 2004). Voronkov and Falster proposed a dissociative model to explain the N diffusion in silicon (Voronkov and Falster 2004), where N transport proceeds via dissociation of the practically immobile dimers into mobile monomers by oxygen catalyzing. Meanwhile, Murphy et al. pointed that the barrier of N monomer should be less than 1.5 eV through experiments on the pinning effect of N on dislocations (Alpass et al. 2009; Murphy et al. 2005). These models are not crucial for photovoltaic level CZ-Si and mc-Si materials.

Nitrogen in Czochralski Silicon

Doping of N in CZ-Si Growth

N-doping in bulk Si is usually achieved by introducing N atoms into molten silicon during crystal growth. Solid and gas N source can be used for constructing N-rich growth environment.

Silicon nitride (Si_3N_4) powders are the most widely used solid N-doping source. The major parameters of the powders are purity and size. The purity of powders should be better than 1 ppm. The powder size is associated with the dissolution rate. Incompletely dissolved powders will usually float above the molten silicon and generate dislocations and even grain boundaries in a CZ-Si ingot (Yu et al. 2011). Si_3N_4 powders can be added to the crucible prior to any heating of polycrystalline silicon (poly-Si) material or during the melting of poly-Si. Another solution is to use

a crucible with Si_3N_4 coating on the inner walls. During the melting process, the Si_3N_4 coating keeps gradually dissolving into the molten silicon, and the N concentration in the molten silicon is determined by convective transport. This makes it difficult to precisely control the doping amount when a N concentration lower than 10^{15} cm^{-3} is needed. So, this technique is usually combined with empirical experience. In addition, boron nitride (BN) powders can also be used as N dopant for *p*-type Si crystal, where the doping amount of B should be well calculated for intended resistivity. BN is more refractory than Si_3N_4 at the melting point of Si so that the powder sizes should be further reduced to assure the complete dissolution of BN in the molten silicon, and meanwhile the melting time should be prolonged.

Nitrogen gas was once considered unable to serve as the protective ambient for CZ-Si growth, because N_2 reacts with polycrystalline silicon (poly-Si) nuggets under high temperature with the regular partial pressure (Kaiser and Thurmond 1959), fierce reaction between solid Si and N_2 generates macroscopic Si_3N_4 particles on the surface of poly-Si and therefore inhibits the growth of defect-free single crystal. The gas doping of N in CZ-Si was first introduced by Que et al. (1985, 1987, 1991, 2000), where N_2 or N_2/Ar mixture under reduced N_2 partial pressure was used as the protective gas, and they successfully obtained N-doped Czochralski silicon (NCZ-Si) ingots. For the growth of NCZ-Si, the purity of protective N_2 atmosphere should be ensured, and the total gas flow rate should be controlled at a relatively high speed to efficiently eliminate SiO vapored above the molten silicon. The doping mechanism is to control the reaction velocity between N_2 and solid poly-Si feedstock by tuning the partial pressure of N_2 . During the melting stage, N_2 reacts with poly-Si, and thin Si_3N_4 film (thickness less than 100 nm) is generated on the surface of poly-Si, and these N contents will completely dissolve in the molten silicon. Therefore, the doping amount can be controlled by manipulating the partial pressure and flow rate of N_2 during the melting stage, instead of during the growth stage. With the decrease of N_2 partial pressure, the chemical reaction of N_2 with poly-Si becomes weak, and therefore, the final N concentration in silicon crystals is controllable. The N concentration in the tail of a CZ-Si is usually less than $5 \times 10^{15} \text{ cm}^{-3}$, due to the liquid solubility and segregation coefficient of N. When the N_2 partial pressure is controlled well, the concentration of N in molten Si will not exceed its solubility, and no Si_3N_4 will float on the liquid surface, so that the CZ growth will not be disturbed, and a high yield of dislocation-free single crystal can be obtained. Considering the low cost of N_2 against Ar, and the benefits of NCZ-Si, using N_2 as the protective atmosphere under reduced pressure has been a cost-effective method for CZ-Si crystal growth.

N-O Complexes

N-O complexes introduce shallow thermal donors in CZ-Si. The ionization of these donors can be characterized by low-temperature FTIR. A typical LT-FTIR spectrum

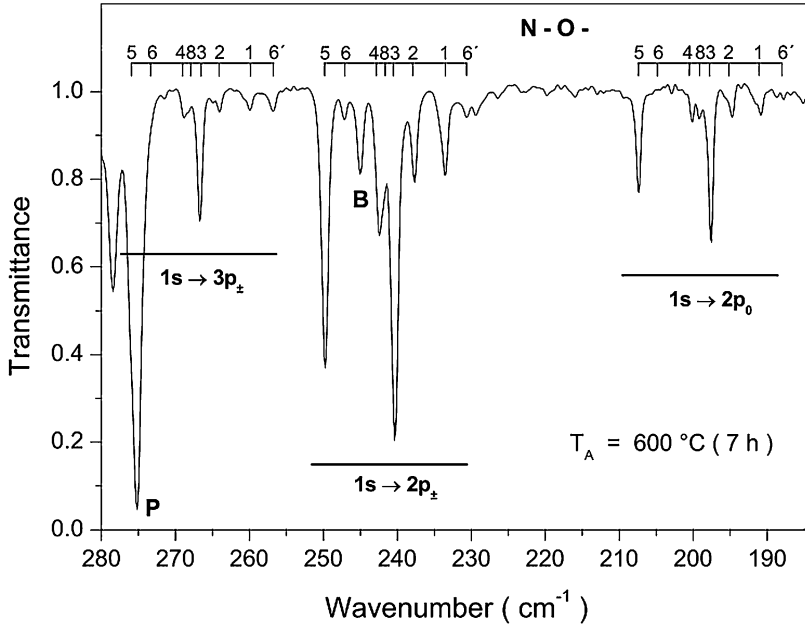


Fig. 2 LT-FTIR (10 K) transmittance spectrum of N-O shallow donors (Alt and Wagner 2010), the absorption peaks correspond to $1s \rightarrow 2p_0$, $1s \rightarrow 2p_{\pm}$, and $1s \rightarrow 3p_{\pm}$, noted by Suezawa et al. (1986) and Wagner et al. (2007)

Table 4 STD absorption peak positions measured at 8 K (Suezawa et al. 1988; Wagner et al. 2007)

Species	$1s \rightarrow 2p_0$ (cm^{-1})	$1s \rightarrow 2p_{\pm}$ (cm^{-1})	$1s \rightarrow 3p_{\pm}$ (cm^{-1})
N-O-1	190.8	233.8	260.1
N-O-2	194.9	237.8	264.2
N-O-3	197.7	240.4	266.8
N-O-4	200.2	242.5	269.0
N-O-5	207.4	249.8	276.4
N-O-6	204.4	247.0	274.2
N-O-6'	187.9	230.6	256.9
N-O-8	199.1	241.5	268.2

of shallow thermal donors (STDs) is shown in Fig. 2 (Alt and Wagner 2010). Three series of bands of the $1s \rightarrow 2p_0$, $1s \rightarrow 2p_{\pm}$, and $1s \rightarrow 3p_{\pm}$ transitions were detected, and eight different species in each band were labeled as N-O- x ($x = 1, 2, 3, \dots$) in Table 4. Several ionization energies of the STDs have been estimated, as shown in Table 5 (Alt and Wagner 2010). There are good agreements between the observed transition energies and the results of the effective mass approximation calculated for the STD states in silicon.

The absorption coefficients of the transitions (N-O-1, N-O-2, N-O-3, N-O-5) increase with the N content in square root dependence (Ewels et al. 1996; Alt

Table 5 Ionization energies of the shallow donors (Wagner et al. 2007)

Donor Groups	Ionization energy (meV)
1	35.38
2	35.90
3	36.21
4	36.45
5	37.38

et al. 2006). According to the mass action law for the reaction $n\text{N} + m\text{O} = \text{N}_n\text{O}_m$, it leads to the integrated absorption values equal to $[\text{N}]^n[\text{O}]^m$. The N predominantly exists in the dimer form, so the concentrations of interstitial N atoms $[\text{N}_i]$ can be expressed as

$$[\text{N}_i] \approx (\rho\text{N}/2)^{1/2} \exp(-E/2kT),$$

where ρ is the lattice site density. Note that the square root dependence is obtained in the expression. This coincidence shows that the STDs should involve only one N atom. The oxygen concentration dependence of the STDs had been investigated by Wagner et al. (2007; Hara et al. 1989). The chemical compositions of the electrically active N-O complexes in silicon were determined in a specially doped ingot with variable oxygen concentrations and a fixed N concentration by FTIR technique. The result shows that the N-O-5, with its absorption at 249.8 cm^{-1} in $1s \rightarrow 2p_{\pm}$ transition, has a linear dependency, proving N-O-5 to be NO ($m = 1$). The other two species of N-O-4 (242.5 cm^{-1}) and N-O-6 (256.9 cm^{-1}) also show the linearity between $[\text{NO}_m]$ and $[\text{O}_i]$; therefore they have the same NO stoichiometry. N-O-3 with its transitions $1s \rightarrow 2p_{\pm}$ at 240.4 cm^{-1} has a square dependence on $[\text{O}_i]$, indicating that it has a NO_2 composition. The power dependency $m = 3$ of the complexes N-O-1 (233.8 cm^{-1}), N-O-2 (237.8 cm^{-1}), and N-O-8 (241.5 cm^{-1}) identifies these STDs as NO_3 defects. The composition of N-O-6 remains unknown.

As N-O complexes are shallow donors in silicon materials, they can influence the resistivity of both p -type and n -type wafers. Therefore, the thermal history of the wafers should be noted during the fabrication of solar cells or electronic devices. N-O complexes in CZ-Si gradually degenerate when the sample is annealed with the temperature higher than $750 \text{ }^{\circ}\text{C}$. The degeneration velocity increases with annealing temperatures, while the formation of N-O complexes happens in the annealing temperature window of $450\text{--}750 \text{ }^{\circ}\text{C}$, when N dimers react with interstitial oxygen and generate N-O complexes. Figure 3 shows the degeneration and regeneration process of N-O complexes in a N-doped CZ-Si sample. The left image shows that the annealing at $850 \text{ }^{\circ}\text{C}$ for 2 h can completely remove the N-O complex-related peaks at $801, 996, \text{ and } 1026 \text{ cm}^{-1}$, and the right image shows that the N dimer peaks at $766 \text{ and } 963 \text{ cm}^{-1}$ decrease the fastest when annealed at $550 \text{ }^{\circ}\text{C}$, and the multiple new peaks are formed during the low-temperature annealing, indicating that the thermal stability of various complexes is different, which means that the degeneration and regeneration of N-O complexes are not absolutely reversible.

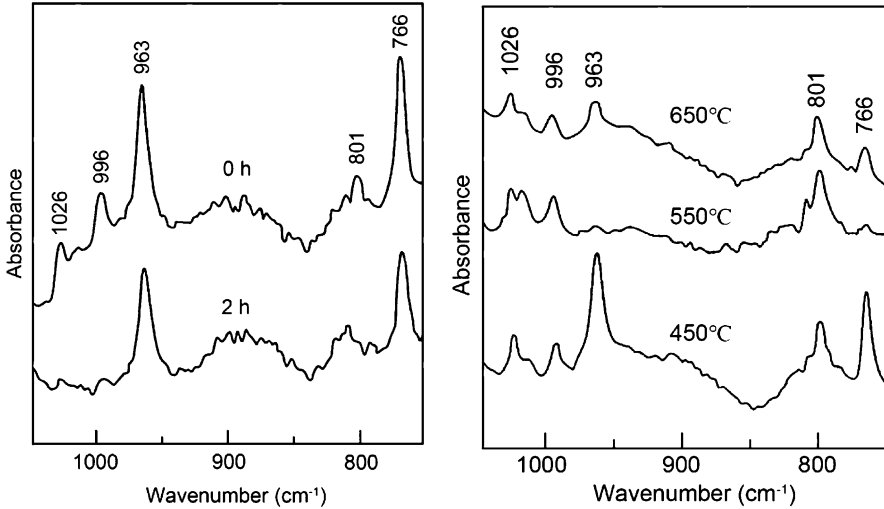


Fig. 3 The FTIR spectra of N-doped CZ-Si (left) before and after annealing at 850 °C for 2 h, (right) annealed at 450, 550, and 650 °C for 24 h after complete N-O complex degeneration

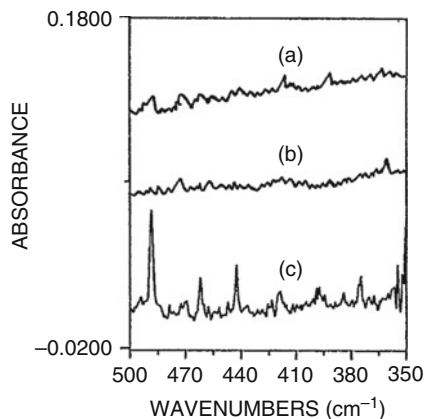
Influence on O-Related Defects

Thermal Donors

Thermal donors (TDs) are usually accumulated from enriched oxygen impurities during the cooling stage of CZ-Si ingots or in the long-time annealing in the temperature of 350–500 °C. TDs are doubly ionized at room temperature and cause downward shift of resistivity in *n*-type phosphorus (P)-doped silicon, which usually introduces two donor levels of $E_c-0.05$ eV and $E_c-0.15$ eV. TDs can be eliminated in the high-temperature courses of normal solar cell processes, i.e., phosphorus diffusion process, so their influence on the performance of wafers and solar cells does not get enough attention. With the developments of high efficiency and low-temperature SHJ solar cell process, this issue starts to become more and more important. Since the maximum temperature of SHJ processes remains below 300 °C, as mentioned above, the as-grown TDs are still retained in the bulk of silicon wafers. TDs have negative influences on the performance of SHJ solar cells. The decrease of minority carrier lifetime is the uppermost factor responsible for the deterioration of efficiency (Li et al. 2018). The results indicate that the solar cell manufacturers should choose the wafer with the concentrations of TDs as low as possible to limit their detrimental effect on the cell efficiency. Furthermore, it is of great importance for silicon crystal growers to manage to reduce the contamination of oxygen during the crystal growth and make the ingot cooling time as short as possible or develop appropriate methods to decrease oxygen concentration and suppress the formation of thermal donors.

Nitrogen has twofold effects on the generation of donors (TDs and STDs) in silicon. As mentioned above, a family of N-O complexes related to both N and O

Fig. 4 LT-FTIR spectra related to thermal donors in CZ-Si. (a) High [N], (b) low [N], (c) N-undoped (Yang et al. 1995)



impurities forms at temperatures around 650 °C, and as a result, the formation of TDs associated only with oxygen impurity is suppressed. Early research identified new STDs (not as N-O complexes) in NCZ-Si using photothermal ionization spectroscopy (PLIS), along with the suppression of the formation of TDs (Griffin et al. 1989). Then using low-temperature far-infrared spectroscopy (LT-FTIR), as shown in Fig. 4, it was found that N suppresses the formation of TDs in CZ-Si annealed at 450 °C, while N interacts with oxygen atoms to form N-O complexes (Yang et al. 1995). The interaction of N and oxygen atoms is supposed to reduce the TDs.

Oxygen Precipitates

Supersaturated interstitial oxygen atoms in CZ-Si can aggregate into oxygen precipitates (OPs) and further induce secondary lattice defects during thermal processing. These defects can getter harmful metal contaminants but induce punch-out dislocations causing the decrease of mechanical strength. The controlling of OPs in CZ-Si is very important for improving performance and yield of ICs. The formation of OPs consists of two stages, i.e., nucleation and growing up. It has been reported that N atoms in CZ-Si can introduce heterogeneous nuclei enhancing the generation of OPs (Karoui and Rozgonyi 2004); therefore, NCZ-Si has been well developed and applied in the IC industry since stronger internal getting is demanded when processing temperatures keeps decreasing (Yang and Yu 2004; Yu et al. 2013).

For solar cells as bulk devices, internal getting on the base of OPs and induced extended defects is not suitable. Moreover, OPs within CZ-Si wafers will introduce deep energy levels in band gap and become the recombination centers for minority carriers, so that the lifetime of wafers decreases. The degree of lifetime degradation was more pronounced in *p*-type silicon than in *n*-type silicon because the recombination of OPs takes place through their interface states, where the existence of positive fixed charges around OPs will boost the lifetime degradation in *p*-type silicon. The performance on *p*-type (Ga-doped) CZ-Si Al-BSF solar cells with intentionally formed OPs shows that the degradation increases sharply with the

concentration of OPs, mainly contributed by the long-wave loss related to bulk recombination (Chen et al. 2011). In fact, the influence of N-related impurities on OPs should be noticed in the cases which the CZ-Si wafers containing high oxygen contents go through long-term annealing. However, currently the fabrication temperature of Al-BSF solar cells is lower than 900 °C, and the annealing time is shorter. Thus, the process does not introduce OPs in solar cells if as-grown oxygen contents are not high enough. Moreover, the N concentration in CZ-Si materials used for photovoltaic industry is very low. Therefore, N-doped CZ-Si could be used for the fabrication of solar cells due to the advantages of low-cost protective gas and higher mechanical strength.

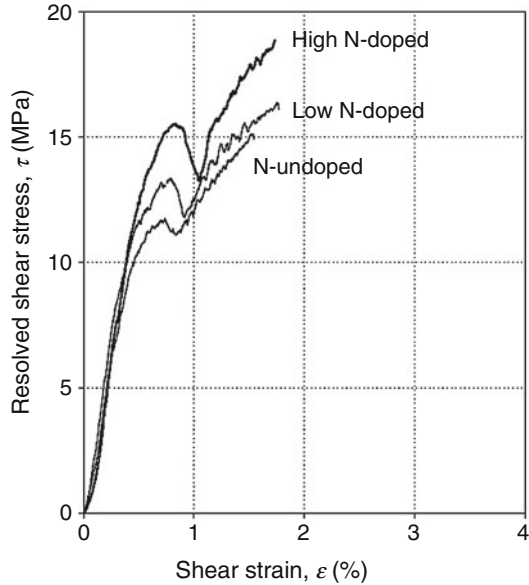
Effect of N Impurity on Mechanical Properties

The mechanical properties of CZ-Si wafers for solar cells are crucial for ensuring manufacturing yield of wafers and cells, especially when the wafer thickness keeps decreasing in recent years. Silicon, as a brittle material at room temperature, is susceptible to breakage or fracture during cell manufacturing due to any localized stress. Generally, the mechanical properties of silicon are dictated by the generation and extension of microcracks, which is related to the generation and motion of dislocations. For CZ-Si, N as co-dopant also affects the mechanical properties of CZ-Si (Lu et al. 1998; Wang et al. 2001; Yu et al. 2013).

The effect of N-doping on Young's modulus and hardness of silicon has been studied by nano-indentation. N-doping with a concentration of $2 \times 10^{15} \text{ cm}^{-3}$ can significantly increase the Young's modulus (from 104 to 182 GPa) and hardness (from 6.49 to 8.11 GPa) of float-zone (FZ) silicon (Anderson 2004). The room temperature fracture strength of N-doped wafers was investigated with a double ring bending setup, where FZ silicon wafers with the low N and O concentration ($< 2 \times 10^{14}$ and $3\text{--}4 \times 10^{15} \text{ cm}^{-3}$, respectively) exhibited a significantly higher fracture strength than conventional CZ ($[\text{O}_i]$: $7.2\text{--}8.6 \times 10^{17} \text{ cm}^{-3}$) or FZ ($[\text{O}_i]$: $4\text{--}15 \times 10^{15} \text{ cm}^{-3}$) wafers, whereas FZ-Si wafers with the high N concentration ($1.7\text{--}3.6 \times 10^{15} \text{ cm}^{-3}$) but without O did not possess the improved fracture strength (Vedde and Gravesen 1996). Besides, for CZ-Si, N-doping can always improve fracture strength. This implies that the improvement in the fracture strength of silicon by N-doping relies on the presence of oxygen. Oxygen precipitates and N-O complexes are suggested to be responsible for the increase in fracture strength for NCZ-Si (Wang et al. 2001; Chen et al. 2008).

Interstitial oxygen can suppress slip and warpage of CZ-Si wafers (Hu and Patrick 1975; Yonenaga et al. 1984). Likewise, interstitial N dimers and N-O complexes have the similar effects. Interestingly, a minor concentration of N ($< 3 \times 10^{15} \text{ cm}^{-3}$) is found to be very effective in reducing slips in low-oxygen content silicon wafers (Wagner et al. 1988). N-doping with a concentration of $3.6 \times 10^{15} \text{ cm}^{-3}$ can reduce wafer warpage of CZ-Si wafers during annealing

Fig. 5 Stress-strain curves of dislocation-free Czochralski silicon crystals deformed in the $\langle 110 \rangle$ direction at 850°C for different N concentrations. The concentrations of N in the samples are 3×10^{13} – $3 \times 10^{14} \text{ cm}^{-3}$ for low N-doped samples, 3×10^{14} – $3 \times 10^{15} \text{ cm}^{-3}$ for high N-doped samples, and $< 3 \times 10^{13} \text{ cm}^{-3}$ for the N-undoped samples (Orlov et al. 2002)



(Lu et al. 1998). Moreover, the dislocation glide around an indentation on CZ-Si at high temperatures is found to be significantly suppressed by N-doping (Hu and Patrick 1975; Yonenaga et al. 1984). In CZ-Si with different N concentrations, an increase in the N concentration leads to enhanced upper and lower yield points, as shown in Fig. 5 (Orlov et al. 2002). This implies that N-doping can increase the tolerable processing temperatures at which the plastic deformation of silicon wafers under load can be avoided. The locking of dislocations by N can be directly evidenced by the increased unlocking stress, which refers to the critical stress for dislocation movement. It is proved that the FZ silicon with higher N concentrations has larger unlocking stresses, implying the increase in N concentration results in a stronger locking effect (Murphy et al. 2006). The interaction energy between N and dislocations has also been studied by measuring the unlocking stress as a function of temperatures (Yonenaga 2005). The experimentally estimated energy for dislocation escaping from the locking of N atom is 4.1 eV, slightly higher than that of 3.6 eV between dislocations and oxygen (Yonenaga et al. 2005). This interaction energy cannot be understood in terms of the model in which the dislocations interact with individual impurity atoms. Consequently, it is proposed that impurity atoms segregate at dislocations and pipe diffuse along the dislocation line, forming complexes or clusters which immobilize dislocations strongly (Yonenaga 2005). Molecular dynamics (MD) modeling suggests that the binding energy of N with edge dislocation (1.66 eV/A $^\circ$) is slightly lower than that of oxygen (1.8 eV/A $^\circ$) (Sumino et al. 1983). In brief, both the experimental and theoretical results agree that N has a strong dislocation locking ability which is comparable with that of oxygen.

Nitrogen in Cast Multicrystalline Silicon

Soluble Nitrogen

Cast multicrystalline (mc-Si) materials used in photovoltaic industry, including quasi-single crystal silicon (QSC-Si) which is also called as mono-like silicon (ML-Si), are fabricated using directional solidification method. In this technology, the size of the crucibles is much larger than that of CZ-Si, and the ingots are directly in contact with the crucible wall. However, the contact of molten silicon and quartz crucibles under high temperatures can cause sticking between them, which generates the crack of ingots during cooling because silicon and quartz have different thermal conductivities. Therefore, Si_3N_4 coating layer (usually a mixture of $\alpha\text{-Si}_3\text{N}_4$ and $\beta\text{-Si}_3\text{N}_4$) on the inner surface of quartz crucibles is usually used to prevent the reaction between molten silicon and crucibles. However, N atoms are induced into mc-Si ingots by the Si_3N_4 coating (Ghosh et al. 1997). And, the convection of molten silicon in large-scale crucibles during the growth of mc-Si is much weaker compared to the growth of CZ-Si, which weakens the segregation of N during solidification. Consequently, the distribution of N-related impurities in cast mc-Si ingots is more complicated than that in N-doped CZ-Si ingots.

N Dimers

The distribution of N concentration in a mc-Si ingot is controlled by both the entrance and segregation of N atoms during the whole growth. For normal cast silicon materials, the only but excessive N source is Si_3N_4 coatings on the inner wall of crucibles. As the diffusivity and temperature is similar, the distribution of N concentration in molten silicon is strongly influenced by the size of crucible, melting time, and convection. Convection is also the main factor controlling the effective segregation. During melting and solidification, Si_3N_4 coating, as the only N dopant, keeps dissolving into the molten silicon; the doping rate is positively correlated with the contacting area between molten silicon and Si_3N_4 coating. Since the temperature and time duration respectively are high and long enough, the N concentration in molten silicon should be at high-level, especially almost saturated for the cases using small crucible, which is close to $6 \times 10^{18} \text{ cm}^{-3}$ as mentioned above.

Small crystals are better for investigating the influence of convection on segregation, where final N concentration in solid phase is usually only controlled by the segregation effect because N is usually well diffused in the molten silicon. Trempa et al. investigated the N distribution in a small ingot with width of 6 cm. Figure 6a shows the axial nitrogen distribution (measured by FTIR) of the central region of ingots. Two ingots (A1 and B1) were grown with enhanced convection using standard Si_3N_4 coating, and in one case (B1) additional Si_3N_4 powders were added to the feedstock and the homogenization time was extended to 10 h. Another two ingots (C1 and D1) used the crucibles with (D1) or without (C1) Si_3N_4 coating. For the process with strong convection (Ingot A1 and B1), nitrogen is axially homogeneously distributed in the range of $(2\text{--}4) \times 10^{15} \text{ cm}^{-3}$ regardless of the adding of Si_3N_4 powders. For moderate convection with Si_3N_4

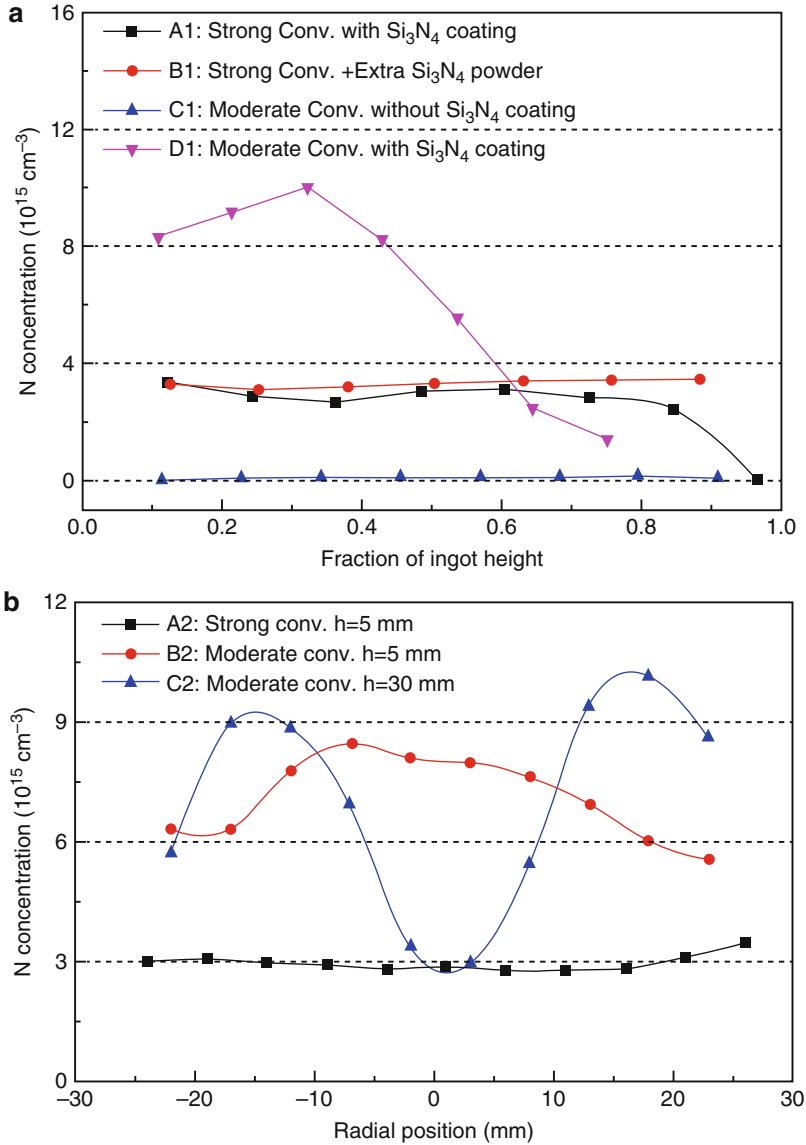


Fig. 6 (a) The axial N concentration in the center of a mc-Si ingot grown in moderate and increased convection with various N sources, (b) the radial N concentration at the height of 5 mm and 30 mm from the bottom of the ingots grown with moderate and increased convection in Si₃N₄-coated crucible. (The data are extracted from Reimann et al. 2010)

coating, Ingot D1, the axial nitrogen concentration keeps increasing at the beginning and reaches to the limit of $1 \times 10^{16} \text{ cm}^{-3}$ at 30% solidified fraction and then decreases to below $2 \times 10^{15} \text{ cm}^{-3}$ at 75% solidified fraction when Si₃N₄ and SiC

precipitates were generated so that the soluble N concentration is reduced. As comparison, the sample grown under moderate convection without a Si_3N_4 crucible coating (ingot C1) has an extremely low nitrogen content below the detection limit of the FTIR measurement of $5 \times 10^{14} \text{ cm}^{-3}$. The radial distribution of N concentration is also strongly dependent on the convection. Figure 6b illustrates the measured radial N distributions at the height of 5 mm (A2, B2) and 30 mm (C2) from the bottom of the ingot. Here two ingots were grown from a pure feedstock in a Si_3N_4 -coated crucible with strong (A2) and moderate (B2, C2) convection. With strong convection (A2), N concentration is homogeneously distributed in the range $(2\text{--}4) \times 10^{15} \text{ cm}^{-3}$, and it holds also at a height of 30 mm for this sample (not shown in Fig. 6). As comparison, in the sample grown under moderate convection (B2), the radial N concentration increases slightly toward the center ($8.5 \times 10^{15} \text{ cm}^{-3}$) from the edge ($6 \times 10^{15} \text{ cm}^{-3}$). At the height of 30 mm, the nitrogen concentration increases from $6 \times 10^{15} \text{ cm}^{-3}$ at the edge to the highest values of $(9\text{--}11) \times 10^{15} \text{ cm}^{-3}$ at about 1/4 and 3/4 positions (C2), and it then rapidly decreased to $3 \times 10^{15} \text{ cm}^{-3}$ at the center because the soluble N impurities have been segregated and become precipitates. Figure 7 shows the IR-transmission images of vertical cross sections of ingots grown with various growth rates, where the high growth rate corresponds to a thick boundary layer width and weak segregation effect. Si_3N_4 precipitates will generate when the soluble N concentration is over the solubility of N.

Once the segregation effect with saturated N in molten silicon is clear, the general situation in larger crystal is easy to discuss. Generally, as the dopant is located at the crucible wall, the distribution of N concentration in molten silicon can be estimated combining diffusion and convection, which means N concentration in the molten silicon usually decreases from the edge toward ingot center, but strong convection and long melting time will reduce the horizontal concentration gradient. During solidification, the distribution of N in solid phase is determined by both the concentration in the molten silicon around the solid-liquid interface and the convection level, of which the latter affects both the effective segregation coefficient and the local enrichment above the growth interface. For the cases with poor convection, the concentration in both solid and local liquid phase might be increased at the same

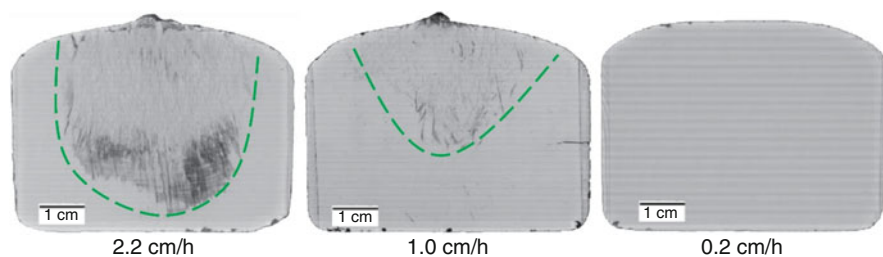


Fig. 7 IR-transmission images of vertical cuts through the ingot center for ingot grown with the growth rate of 2.2, 1.0, and 0.2 cm/h (Trempa et al. 2010)

time. Si_3N_4 precipitates will generate in various forms when the concentration exceeds solubility (see the section “Silicon Nitride Precipitates”). If the convection is strong enough, the N concentration of most parts of the ingot will be stable.

N-O Complex

The formation of N-O complexes requires adequate N and O concentrations. Currently, the N and O_i concentrations in industrial mc-Si ingot are in the range of $4\text{--}6 \times 10^{15} \text{ cm}^{-3}$ and $0.5\text{--}5 \times 10^{17} \text{ cm}^{-3}$, respectively, enough for the formation of N-O complexes. The LT-FTIR absorption peaks of N-O complexes can be easily observed in *n*-type mc-Si (Ghosh et al. 1997). As the N concentration is relatively stable among the whole mc-Si ingot, the formation of N-O complexes is mainly determined by the concentration of interstitial O_i , which depends on the coating selection and decreases along the ingot height. Therefore, the generation of N-O complexes in mc-Si changes with the O_i concentration. It was reported that in *n*-type mc-Si, the fraction of N-O complexes in total soluble N-related impurities can be up to $\sim 44\%$ when $[\text{O}_i] = 3.2 \times 10^{17} \text{ cm}^{-3}$, but smaller than 10% when $[\text{O}_i] < 1.0 \times 10^{17} \text{ cm}^{-3}$ (Zhang et al. 2013). As a result, the distribution of N dimers and N-O complexes in mc-Si is complementary, determined by the distribution of interstitial oxygen O_i , that is, the fraction of dimers is higher at ingot top, while the complexes higher at bottom, as shown in Fig. 8 (Kusunoki et al. 2011).

The common shallow thermal donor (STD) concentration in *n*-type mc-Si was measured as $\sim 1 \times 10^{14} \text{ cm}^{-3}$ (Zhang et al. 2013), which is believed to be caused by N-O complexes. To date, the majority of industrial mc-Si ingots are B-doped *p*-type Si, where the B concentration is about 10^{16} cm^{-3} , so N-O complex STDs with a concentration of $\sim 10^{14} \text{ cm}^{-3}$ should not obviously affect the resistivity of *p*-type wafers. Moreover, the majority of N-O complexes can be eliminated during the P diffusion process (under $800\text{--}900^\circ\text{C}$), so that the influence of N-O complexes on the performance of *p*-type mc-Si solar cell is usually ignored.

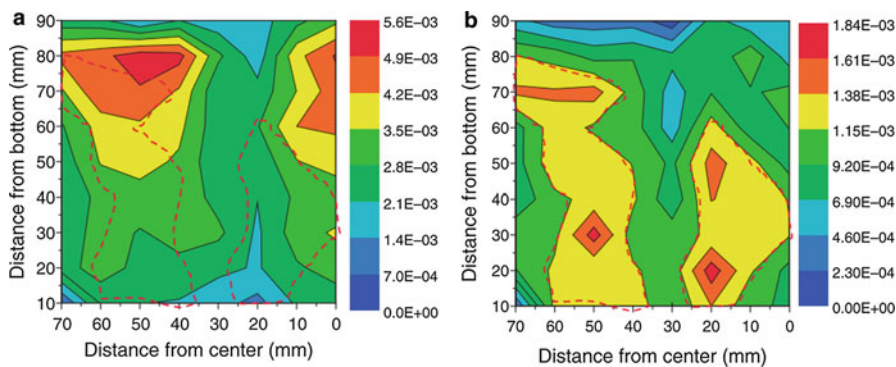


Fig. 8 Complementary distributions of the absorption peak intensities of (a) NN (963 cm^{-1}) and (b) NNO (996 cm^{-1}) over a vertical cross section of mc-Si brick (Kusunoki et al. 2011)

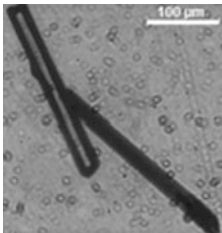
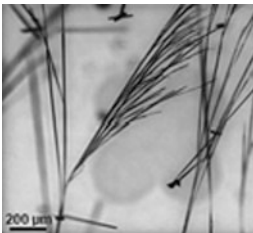
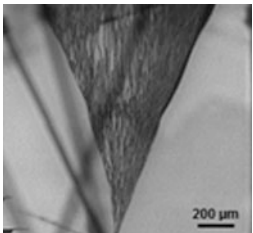
Silicon Nitride Precipitates

Formation

The formation of nitrogen-related precipitates strongly depends on the local thermodynamic conditions and impurity transportation during crystallization. As mentioned, the solubility of N in mc-Si is $\sim 10^{16} \text{ cm}^{-3}$, and Si_3N_4 precipitates are segregated when the local concentration exceeds the solubility. The N concentration in mc-Si at the solid-liquid interface is determined by the effective segregation of N, which is dependent on equilibrium segregation coefficient and convection specifying how heat and mass transfer can take place between liquid and solid interface of silicon. If local N concentration exceeds the liquid solubility, Si_3N_4 precipitates will generate at the liquid part of the interface and sink into the solid phase. Then it has a probability to serve as a seed for further growth of Si_3N_4 crystal; thus, the convection has an important influence to determine how much N content can be transported nearby, which determines the final size of the precipitates. As a result, the common forms of Si_3N_4 precipitates in mc-Si include rods, fibers, and nets, the parameters of which are listed in Table 6 (Richter et al. 2017).

Si_3N_4 rods have relatively large diameter and small length and are perfectly grown as hexagonal, showing no position preference within the grain structure. It indicates that they are grown in liquid Si where the surrounding influence is much lower than that in solid phase. Poor convection could be the main reason for the

Table 6 Classification of Si_3N_4 precipitates in cast mc-Si crystals (Richter et al. 2017)

	Si_3N_4 rod	Si_3N_4 fiber	Si_3N_4 net
Morphology and phase	 Monocrystalline $\beta\text{-Si}_3\text{N}_4$	 Monocrystalline $\alpha\text{-Si}_3\text{N}_4$	 Multicrystalline $\alpha\text{-Si}_3\text{N}_4$
Size (d: diameter, l: length)	d: $< 30 \mu\text{m}$ l: $< 2 \text{ mm}$	d: $< 500 \text{ nm}$ l: $< 8 \text{ mm}$	d: $< 500 \text{ nm}$ l: $< 3 \text{ mm}$
Growth preference	In grain, random	In grain, growth direction	At GB, growth direction
Structure space group lattice constant (nm)	Hexagonal P63 (173) $a = 0.760$ $c = 0.291$	Trigonal P31c (159) $a = 0.775$ $c = 0.562$	Trigonal P31c (159) $a = 0.775$ $c = 0.562$
Impurities, resistance ($\Omega \text{ cm}$)	Li, C, O, Mg, Ca $> 4.7 \times 10^7$	C, O, Ca $(5 \pm 4) \times 10^8$	C, O, Al, Ca $(1.44 \pm 0.26) \times 10^{10}$

formation of Si_3N_4 rods, when the N concentration in molten silicon is relatively high and the convection is relatively poor; most of the segregated N into the molten silicon cannot be transported away, once the concentration exceeds the solubility, and precipitates will be generated in the liquid phase. Because poor convection usually corresponds to fast growth and Si_3N_4 has a higher density (3.44 g/cm^3) than liquid Si (2.55 g/cm^3), Si_3N_4 rods can sink to the solid-liquid interface and get embedded in the solid phase.

Si_3N_4 fibers grow in vertical growth direction within grain. Compared to Si_3N_4 rods, they have obviously longer length and shorter diameter, which indicates that the fibers grow along with the silicon crystal so that the diameter of the fibers is limited and the length prolonged. Therefore, it can be assumed that Si_3N_4 fibers need seeds to start the growth. The equilibrium state of Si_3N_4 inclusion is β phase, while Si_3N_4 fibers show trigonal α - Si_3N_4 crystallographic structure, and they grow in preferred orientation. So far, there is no clear evidence that Si_3N_4 fibers start from Si lattice; some results show that the fibers start from a Si_3N_4 rod inclusion (Li et al. 2013). Consider that the lattice constant of trigonal α - Si_3N_4 ($a = 0.775 \text{ nm}$ and $c = 0.562 \text{ nm}$), close to the hexagonal β - Si_3N_4 ($a = 0.760 \text{ nm}$), and Si lattice constant ($a = 0.543 \text{ nm}$), the lattice mismatch between the fiber seed and β - Si_3N_4 or Si, are both relatively low; therefore, it can be inferred that the seed of Si_3N_4 fibers should be generated at some tensile zone or precipitates enlarging the lattice constant.

Si_3N_4 nets are likewise α phase precipitates but multicrystal found at grain boundaries (GBs). GBs can offer more nucleation sites for the segregation of α - Si_3N_4 , and then a series of fibers can grow within the preferential angle. Si_3N_4 fibers and nets are usually found parallel in one ingot, indicating they are same kind of inclusions with different nucleation sites. The extension of Si_3N_4 fibers/nets is strongly related to the transportation of N content, which is mainly determined by the convection details, and the butterfly shaped nets shown in Fig. 9 are an example to show the complexity of defect extension.

Influence on Wafering and the Mechanical Strength of Wafers

The wafering of mc-Si bricks mainly uses SiC slurry wire sawing in the past several decades, and now the wafering technique has been mostly changed to diamond wire sawing (DWS). As SiC particles are usually generated along with Si_3N_4 precipitates, the influence of SiC and Si_3N_4 precipitates on the mechanical properties should be considered together.

The embedded inclusions such as Si_3N_4 precipitates are harder than silicon bulk. Thus, for wire saw wafering process, the un-uniformed hardness of the Si material introduces local tensile stress on the wire and may cause wire rupture during cutting. Table 7 gives the hardness values of Si, SiC, α - Si_3N_4 , β - Si_3N_4 , and Fe-decorated β - Si_3N_4 (Richter et al. 2017). It is clear that the SiC and Si_3N_4 precipitates are harder than Si, which means they introduce extra local tensile stress on the wire. Despite β - Si_3N_4 is harder than SiC, it should be mentioned that the main form of Si_3N_4 in mc-Si is Fe-decorated β - Si_3N_4 rods (Buonassisi et al. 2006) and the hardness of

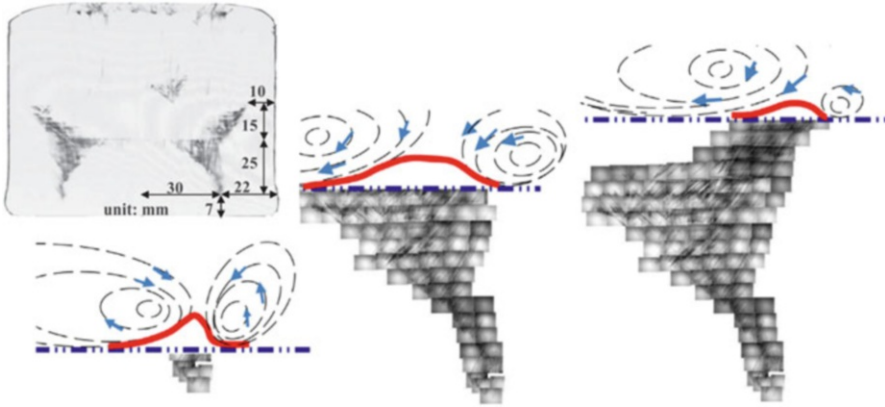


Fig. 9 IR-transmission image of vertical cross section of the ingot with butterfly-shaped Si_3N_4 precipitates and schematic diagram of the convection fluctuation model during the formation (Li et al. 2013)

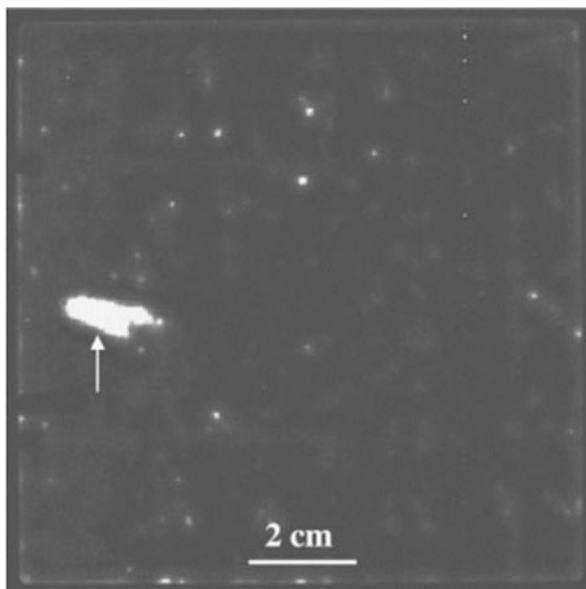
Table 7 Vickers hardness of Si, SiC, $\alpha\text{-Si}_3\text{N}_4$, $\beta\text{-Si}_3\text{N}_4$, and Fe-decorated $\beta\text{-Si}_3\text{N}_4$

	Vickers hardness (GPa)
Si	13 ± 1 (20 mN load) Vandeperre et al. (2007)
SiC	23 ± 2 Snead et al. (2007)
$\alpha\text{-Si}_3\text{N}_4$	~ 38 (200 g load) Chakraborty and Mukerji (1980)
$\beta\text{-Si}_3\text{N}_4$	~ 30 (200 g load) Chakraborty and Mukerji (1980)
$\beta\text{-Si}_3\text{N}_4$ with 0.1 wt% Fe	~ 19 (200 g load) Chakraborty and Mukerji (1980)

$\beta\text{-Si}_3\text{N}_4$ can be reduced by Fe decoration, lower than the value of SiC but still higher than Si (Chakraborty and Mukerji 1980). Therefore, it is believed that SiC particles and filaments are the major hard inclusions in mc-Si. This supports the fact that the $\beta\text{-Si}_3\text{N}_4$ rods and very thin $\alpha\text{-Si}_3\text{N}_4$ are usually easily cut during wafering. However, hard SiC particles are usually highly localized around $\beta\text{-Si}_3\text{N}_4$ rods. Therefore, the existence of SiC and Si_3N_4 precipitates is the main factor of wire rupture (Du et al. 2007, 2008).

Furthermore, embedded SiC and Si_3N_4 precipitates in mc-Si wafers also decrease the mechanical strength and increase fracture rate of wafers and devices. The adjacent phases have different thermal expansion coefficients (TEC) (Schoenfelder et al. 2009), and the mismatch of the TECs at the interface of precipitates introduces shear stress. The average tensile shear stresses at $\beta\text{-SiC/Si}$ and $\beta\text{-Si}_3\text{N}_4\text{/Si}$ interfaces were reported as ~ 24 and ~ 12 MPa, respectively, measured by infrared birefringence imaging (IBI) (Ganapati et al. 2010). Therefore, when the amount of SiC/ Si_3N_4 precipitates increases, the heterogeneous degree of local tensile stresses will be increased with enlarged net local shear stress, and the probability of stress concentration is increased, which finally leads to the reduction of wafer fracture strength as the critical stress is more easily reached under same load.

Fig. 10 Lock-in thermogram of a cell containing a Si_3N_4 inclusion (arrow) (Breitenstein et al. 2004)



Influence on Electric Properties of Cell Performance

The length of Si_3N_4 inclusions in mc-Si ingots is usually several millimeters, so they commonly penetrate the wafers (width from 160 to 180 μm). Despite the resistivity of penetrating Si_3N_4 is relatively high (Bauer et al. 2007), these inclusions can still serve as shunts in solar cells under forward bias (Breitenstein et al. 2004), as shown in Fig. 10. Generally, it is considered as shunts that cause degradation in fill factor (FF) and open-circuit voltage (V_{oc}). However, for the industrial-level mc-Si cells, the series resistance of the devices cannot be ignored, and then the increase in shunts can also reduce the short-circuit current (J_{sc}) at the same time. Meanwhile, Si_3N_4 inclusions are the nucleation sites for SiC particles. Penetrating SiC filaments at grain boundaries are confirmed low-resistivity shunts, but the size of SiC particles is usually smaller compared to wafer thickness, and $\sim 80\%$ wt of the inclusions have a diameter between 75 and 385 μm (Søiland et al. 2004).

Growth of Multicrystalline Silicon in Ambient Nitrogen

Gas Doping of N for Cast Mc-Si

N-doping through utilizing ambient nitrogen (Yang et al. 2009) has been well applied in CZ-Si growth. NCZ-Si wafers have multiple benefits and features for IC industry, i.e., it provides the flexibility in controlling oxygen precipitates,

suppressing void defects related to vacancies, and improving mechanical strength of wafers. However, for cast mc-Si (including QSC-Si), these features are not as important as for CZ-Si, and certain amounts of N content are incorporated into the crystal due to the reaction of the coated Si_3N_4 on the inner walls of crucible with molten silicon (Ghosh et al. 1997), so there are few interests on gas doping of N for mc-Si. To date, mc-Si ingots are mostly grown in ambient argon.

As discussed above, the N concentration in the molten silicon is relatively high, the ideal segregation coefficient of N in silicon is as small as 7.5×10^{-4} , and the most important, the manufacturers usually do not intentionally change the convection level. Thus, the common range of N concentration in a regular mc-Si ingot is $4\text{--}6 \times 10^{15} \text{ cm}^{-3}$. And the soluble N concentration in the mc-Si crystal must be controlled lower than 10^{16} cm^{-3} in solid phase, or else Si_3N_4 precipitates must be generated and then cause dense defects in silicon crystal.

When casting mc-Si ingots in ambient nitrogen, additional N sources are introduced in the system as Si_3N_4 film or particles, and they are generated at the solid Si surface by the reaction between polycrystalline Si and N_2 during the melting stage. Because the convection in casting method is much lower compared with CZ growth, the additional Si_3N_4 generated on poly-Si nuggets increases the contact area between Si_3N_4 and molten silicon, which increases the localized N concentration in both liquid and solidified silicon. Once the N concentration is oversaturated, Si_3N_4 precipitation should be generated in the crystal. Figure 11 shows the minority lifetime mapping images of mc-Si ingots grown in Ar (MC), N_2 with (NMC1) reduced and (NMC0) regular pressure. The inset of Fig. 11 shows the Si_3N_4 precipitates and related cracks in the ingot MNC0 grown in ambient N_2 with regular pressure of 600 mbar. The mapping of brick shows that the relatively high N_2 partial pressure can cause many cracks in the crystal. These cracks are filled with Si_3N_4 precipitates, and dense dislocations/grain boundaries are generated nearby. SEM photo shows that the precipitates are mostly needle-like, suggesting that they are $\beta\text{-Si}_3\text{N}_4$, which means they are not unmelted coating because the coating is usually

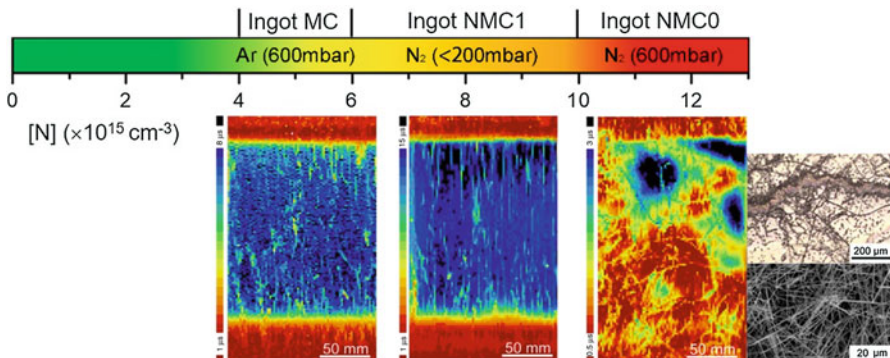


Fig. 11 The minority carrier lifetime mapping of mc-Si grown in Ar (MC), N_2 with reduced pressure (NMC1) and normal pressure (NMC0). Inset shows the defect distribution near a crack shown by Secco etching and SEM photo of Si_3N_4 precipitates located in the cracks

composed by α - Si_3N_4 . Meanwhile, Si_3N_4 particles formed before solidification will float upward the surface of the molten silicon and cannot exist in the bulk. The generation of cracks should be related to the high thermal stress after solidification during the hot temperature phase of crystal growth, the fast diffuser N-N pairs could diffuse to the crack surfaces and then form silicon nitride particles. However, the detailed mechanism for the formation of the cracks with silicon nitride aggregation still needs more experiments to reveal.

The N concentration can be controlled through manipulating N_2 partial pressure. Fine mc-Si ingots can be obtained under ambient nitrogen with reduced pressure. The total N concentration in the top samples was measured to be $9.4 \times 10^{15} \text{ cm}^{-3}$ by SIMS, which is much higher than the regular range of $4\text{--}6 \times 10^{15} \text{ cm}^{-3}$. This indicates that the N concentrations can be effectively improved by the utilization of ambient nitrogen with a reduced pressure. Figure 11 also shows that the minority carrier lifetime of NMC0 is lower than that of NMC1 due to the generation of massive cracks, and the carrier lifetime of NMC1 is even better than MC. This suggests that the increase in N concentrations up to $9.4 \times 10^{15} \text{ cm}^{-3}$ has no influence on the carrier recombination properties of cast mc-Si materials and, therefore, should do no harm on the performance of solar cells.

Improvement in Mechanical Strength

It is well known that the introduction of N can enhance the mechanical strength of CZ-Si (Wang et al. 2001); therefore, the extra N-doping in mc-Si can likewise further enhance the fracture strength of wafers. The influence of extra N-doping on fracture strength is investigated using twist breakage test combined with Weibull analysis. Twist test is the most widely used tool to characterize the fracture strength, considering the nonuniform grain structure of mc-Si wafers. Figure 12 shows the scheme of twist test for $156 \times 156 \text{ mm}^2$ wafers, where wafers were placed on fixed lower dowel

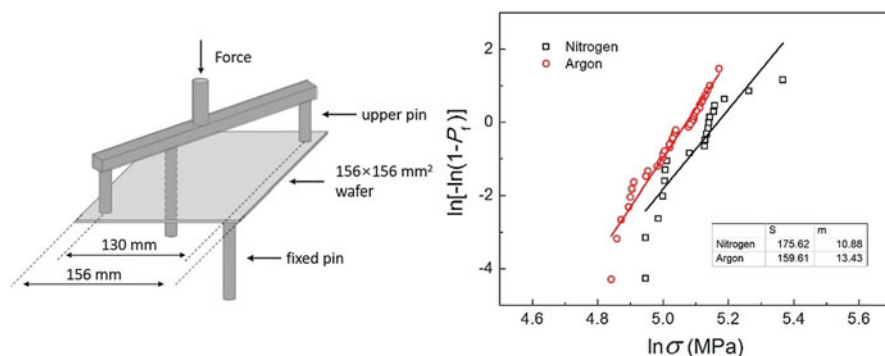


Fig. 12 Schematic setup of the twist-test configuration and the Weibull plots of the variation of fracture strength with the applied stress for the wafers from the ingots grown in N_2 and Ar (Yuan et al. 2018)

pins and the upper dowel pins move downward until they reach the wafer surface, and then loads are applied by upper pins moving downward on the unsupported corners of the wafers until the breakage. Nevertheless, the stress distribution of twist test is nonlinear (Schoenfelder et al. 2007), and a characteristic fracture strength value can be defined as $\sigma = CFb/d^2$ for evaluation, where C is a constant (C was set as 2 in this work), F is the fracture force, d the wafer thickness, and l and b the geometric parameters for wafer and tester, which are 156 and 130 mm, respectively. The Weibull method describes the failure probability as a function of strength,

$$P_f = 1 - \exp[-(\sigma/\sigma_0)^m],$$

where P_f is the failure probability at the applied stress σ and σ_0 and m are defined as the characteristic strength and the Weibull modulus, respectively. $P_f = (n - 1/2)/N$, dependent on its ranking number, n (N is the total number of samples). σ_0 equals to the stress when 63% of all samples fail and m describes the variability of strength data. High m value means smaller scattering of σ . Therefore, through a linear fit of $\ln(-\ln(1 - P_f))$ versus $\ln \sigma$, σ_0 and m can be determined from the slope and intercept. Figure 12 also shows the Weibull distribution of the fracture strength of wafers from the ingots grown in N_2 and Ar, the total number of wafers is 36 and 37, and the characteristic strengths are 175.62 and 159.61 MPa, respectively. It is clear that the wafers from the ingot grown in nitrogen are statically harder.

Impact of N-O Complexes in Mc-Si Grown in Ambient N_2

The increase in N concentration in mc-Si grown in ambient N_2 may cause increase in N-O concentration. N-O complexes introduce shallow thermal donors (STD) in silicon and may cause compensation in p -type mc-Si. As mentioned above, the fraction range of N-O complexes in mc-Si is 10–40% considering O_i concentration; therefore, when the total N concentration reaches $\sim 10^{16} \text{ cm}^{-3}$, the STD concentration can be higher than 10^{15} cm^{-3} , when the influence on resistivity cannot be easily ignored.

Figure 13a shows the resistivity distribution of ingots grown in N_2 and Ar along the ingot height. It is interesting that the resistivity of N-doped ingot grown in N_2 increases with ingot height, while that of the referential ingot grown in Ar decreases normally. Since the boron doping is same for both ingots, the difference in resistivity distribution between the two ingots is attributed to the formation of N-O complexes, which serve as shallow donors and compensate boron acceptors (Yang et al. 1996). Note that N-O complexes also exist in normal mc-Si grown in argon, and they are commonly eliminated during phosphorus diffusion process (by annealing under 800–900 °C for ~30 min) so that the substrate material of final Al-BSF solar cell is not compensated. Figure 13b shows the resistivity variation of samples sliced from the top of N-doped and referential ingots, after the annealing under 900 °C and then 650 °C to degenerate and regenerate N-O complexes, respectively. The corresponding interstitial oxygen concentration at the ingot top is measured to be

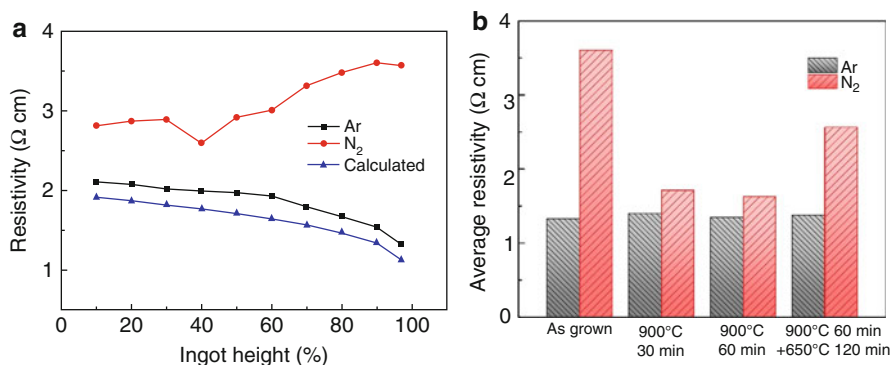


Fig. 13 (a) The resistivity distribution of B-doped p-type ingots grown in N_2 and Ar ambient versus various ingot heights. (b) The variation of average resistivity of top samples from the ingots grown in N_2 and Ar after various thermal annealings (Yuan et al. 2018)

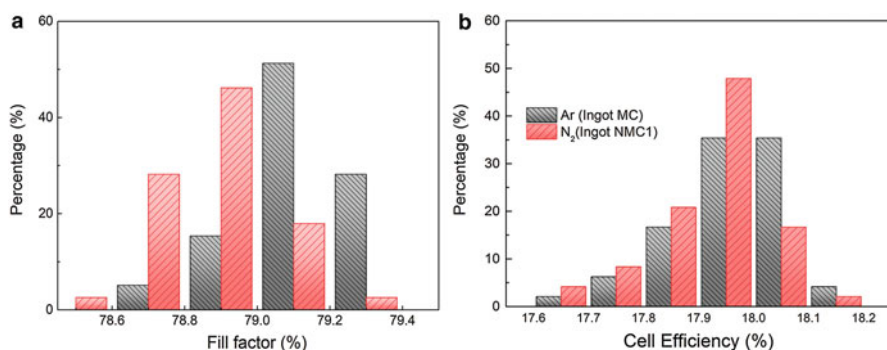


Fig. 14 (a) Fill factor distribution of solar cells. (b) The resistivity variation after heat treatment of top samples sliced from ingot NMC1 and ingot MC (Yuan et al. 2018)

$\sim 6.8 \times 10^{16} \text{ cm}^{-3}$ by FTIR. The resistivity of the N-doped sample obviously decreases when annealed under 900 °C and increases when latterly annealed under 650 °C. It can be explained by the degeneration and regeneration of N-O complexes in N-doped samples.

Standard Al-BSF solar cells based on wafers from the ingot grown in N_2 with reduced pressure were fabricated. Since it has been shown that thermal annealing in Al-BSF cell manufacturing cannot totally eliminate N-O complex shallow donors, then the bulk resistivity of NMC1 wafers is higher than the reference after annealing under 900 °C, which causes higher series resistivity and lower fill factor of the solar cells. The distributions of fill factor values are shown in Fig. 14a. As a result, Fig. 14b shows the distribution of solar cell efficiencies for both kinds of the wafers. The average efficiencies are almost the same for the solar cells based on the ingot NMC1 and MC, which are 17.91% and 17.96%, respectively. This indicates that the high concentration of nitrogen has a little influence on solar cell performances. It can

be inferred that a better overall resistivity distribution of the whole ingot can be obtained if N-O complex-related compensation is well controlled. For the consideration of application of N-doped silicon, an additional B doping should be adopted to fit the cell manufacturing process.

Conclusion

This chapter reviews the basic properties of nitrogen in photovoltaic silicon materials. The development of N-doped CZ-Si wafers is crucial for IC industry. As NCZ-Si has not been widely used in photovoltaic fields, related knowledge from the perspective of possible photovoltaic application are introduced. As mc-Si, nitrogen impurity is important subject in casting method due to Si_3N_4 -coated crucibles. The concepts of the existence, transportation, and influence of N-related defects are introduced and described to the readers to help understand the relevant phenomena during the solidification process. Finally, cheaper ambient nitrogen for casting multicrystalline silicon ingots has been achieved with comparable crystal quality and solar cell conversion efficiency.

Cross-References

- ▶ [Carbon Impurity in Crystalline Silicon](#)
- ▶ [Grain Boundaries in Multicrystalline Silicon](#)
- ▶ [Growth of Crystalline Silicon for Solar Cells: Czochralski Si](#)
- ▶ [Growth of Crystalline Silicon for Solar Cells: Mono-Like Method](#)
- ▶ [Growth of Multicrystalline Silicon for Solar Cells: Dendritic Cast Method](#)
- ▶ [Growth of Multicrystalline Silicon for Solar Cells: The High-Performance Casting Method](#)

Acknowledgments The authors would like to thank the financial support from the National Natural Science Foundation of China (Nos. 51532007, 61721005). It was also partly supported by Key Project of Zhejiang Province (No. 2018C01034).

References

- C. Alpass, J. Murphy, R. Falster, P. Wilshaw, Nitrogen in silicon: diffusion at 500–750 °C and interaction with dislocations. *Mater. Sci. Eng. B* **159**, 95–98 (2009)
- H.C. Alt, H. Wagner, Piezospectroscopy of nitrogen-oxygen shallow donor complexes in silicon. *Phys. Rev. B* **82**(11), 115203 (2010)
- H.C. Alt, Y. Gomeniuk, F. Bittersberger, A. Kempf, D. Zemke, Analysis of electrically active N-O complexes in nitrogen-doped CZ silicon crystals by FTIR spectroscopy. *Mater. Sci. Semicond. Process.* **9**(1–3), 114–116 (2006)
- P.M. Anderson, in *Nanoscale Materials and Modeling – Relations Among Processing, Microstructure and Mechanical Properties: Symposium* held April 13–16, 2004, San Francisco, California, vol 821. Materials Research Society

- J. Bauer, O. Breitenstein, J.P. Rakotoniaina, Electronic activity of SiC precipitates in multicrystalline solar silicon. *Phys. Status Solidi A* **204**(7), 2190–2195 (2007)
- O. Breitenstein, J. Rakotoniaina, M.H. Al Rifai, M. Werner, Shunt types in crystalline silicon solar cells. *Prog. Photovolt. Res. Appl.* **12**(7), 529–538 (2004)
- P.H. Bucksbaum, J. Bokor, Rapid melting and regrowth velocities in silicon heated by ultraviolet picosecond laser pulses. *Phys. Rev. Lett.* **53**(2), 182 (1984)
- T. Buonassisi, A.A. Istratov, M. Pickett, J.-P. Rakotoniaina, O. Breitenstein, M.A. Marcus, S.M. Heald, E.R. Weber, Transition metals in photovoltaic-grade ingot-cast multicrystalline silicon: assessing the role of impurities in silicon nitride crucible lining material. *J. Cryst. Growth* **287**(2), 402–407 (2006)
- D. Chakraborty, J. Mukerji, Characterization of silicon nitride single crystals and polycrystalline reaction sintered silicon nitride by microhardness measurements. *J. Mater. Sci.* **15**(12), 3051–3056 (1980)
- J. Chen, D. Yang, X. Ma, Z. Zeng, D. Tian, L. Li, D. Que, L. Gong, Influence of germanium doping on the mechanical strength of Czochralski silicon wafers. *J. Appl. Phys.* **103**(12), 123521 (2008)
- L. Chen, X. Yu, P. Chen, P. Wang, X. Gu, J. Lu, D. Yang, Effect of oxygen precipitation on the performance of Czochralski silicon solar cells. *Sol. Energy Mater. Sol. Cells* **95**(11), 3148–3151 (2011). <https://doi.org/10.1016/j.solmat.2011.06.044>
- A. Clark, J.D. Macdougall, K.E. Manchester, P. Roughan, F. Anderson, *Nitrogen Donor Level in Silicon*, Bulletin of the American Physical Society, vol 3 (American Institute of Physics Circulation and Fulfillment Division, Woodbury, 1968), p. 376
- G. Du, L. Zhou, P. Rossetto, Y. Wan, Hard inclusions and their detrimental effects on the wire sawing process of multicrystalline silicon. *Sol. Energy Mater. Sol. Cells* **91**(18), 1743–1748 (2007)
- G. Du, N. Chen, P. Rossetto, Wire-sawing defects on multicrystalline silicon wafers grown by a directional solidification method. *Semicond. Sci. Technol.* **23**(5), 055011 (2008)
- C. Ewels, R. Jones, S. Öberg, J. Miro, P. Deak, Shallow thermal donor defects in silicon. *Phys. Rev. Lett.* **77**(5), 865 (1996)
- N. Fujita, R. Jones, J. Goss, P. Briddon, T. Frauenheim, S. Öberg, Diffusion of nitrogen in silicon. *Appl. Phys. Lett.* **87**(2), 021902 (2005)
- V. Ganapati, S. Schoenfelder, S. Castellanos, S. Oener, R. Koepge, A. Sampson, M.A. Marcus, B. Lai, H. Morhenn, G. Hahn, Infrared birefringence imaging of residual stress and bulk defects in multicrystalline silicon. *J. Appl. Phys.* **108**(6), 063528 (2010)
- M. Ghosh, D. Yang, A. Lawrenz, S. Riedel, H. Moller, Investigation of minority carrier lifetime degradation in multicrystalline silicon ingots, in *Proceedings of the 14th European Photovoltaic Solar Energy Conference*, (1997), pp. 724–727
- J. Goss, I. Hahn, R. Jones, P. Briddon, S. Öberg, Vibrational modes and electronic properties of nitrogen defects in silicon. *Phys. Rev. B* **67**(4), 045206 (2003)
- J. Griffin, J. Hartung, J. Weber, H. Navarro, L. Genzel, Photothermal ionisation spectroscopy of oxygen-related shallow defects in crystalline silicon. *Appl. Phys. A*. **48**(1), 41–47 (1989)
- A. Hara, T. Fukuda, T. Miyabo, I. Hirai, Electron spin resonance of oxygen-nitrogen complex in silicon. *Jpn. J. Appl. Phys.* **28**(1R), 142 (1989)
- P. Hemment, R. Peart, M. Yao, K. Stephens, R. Chater, J. Kilner, D. Meekison, G. Booker, R. Arrowsmith, High quality silicon on insulator structures formed by the thermal redistribution of implanted nitrogen. *Appl. Phys. Lett.* **46**(10), 952–954 (1985)
- R. Hockett, Anomalous diffusion of nitrogen in nitrogen-implanted silicon. *Appl. Phys. Lett.* **54**(18), 1793–1795 (1989)
- R. Hockett, D. Sams, The measurement of nitrogen in silicon substrates by SIMS, in *Proceedings-SPIE the International Society for Optical Engineering, 2000*, (International Society for Optical Engineering, 1999), pp. 584–595
- S. Hu, W. Patrick, Effect of oxygen on dislocation movement in silicon. *J. Appl. Phys.* **46**(5), 1869–1874 (1975)
- T. Itoh, T. Abe, Diffusion coefficient of a pair of nitrogen atoms in float-zone silicon. *Appl. Phys. Lett.* **53**(1), 39–41 (1988). <https://doi.org/10.1063/1.100116>
- Y. Itoh, T. Nozaki, T. Masui, T. Abe, Calibration curve for infrared spectrophotometry of nitrogen in silicon. *Appl. Phys. Lett.* **47**(5), 488–489 (1985)

- R. Jones, C. Ewels, J. Goss, J. Miro, P. Deak, S. Oberg, F.B. Rasmussen, Theoretical and isotopic infrared absorption investigations of nitrogen-oxygen defects in silicon. *Semicond. Sci. Technol.* **9**(11), 2145 (1994a)
- R. Jones, S. Öberg, F.B. Rasmussen, B.B. Nielsen, Identification of the dominant nitrogen defect in silicon. *Phys. Rev. Lett.* **72**(12), 1882 (1994b)
- W. Kaiser, C. Thurmond, Nitrogen in silicon. *J. Appl. Phys.* **30**(3), 427–431 (1959)
- A. Karoui, G. Rozgonyi, Oxygen precipitation in nitrogen doped Czochralski silicon wafers. II. Effects of nitrogen and oxygen coupling. *J. Appl. Phys.* **96**(6), 3264–3271 (2004)
- H. Kusunoki, T. Ishizuka, A. Ogura, H. Ono, Complementary distribution of NN and NNO complexes in cast-grown multicrystalline silicon for photovoltaic cells. *Appl. Phys. Express* **4**(11), 115601 (2011)
- J. Li, R.R. Prakash, K. Jiptner, J. Chen, Y. Miyamura, H. Harada, K. Kakimoto, A. Ogura, T. Sekiguchi, Butterfly-shaped distribution of SiN_x precipitates in multi-crystalline Si for solar cells. *J. Cryst. Growth* **377**, 37–42 (2013)
- J. Li, X. Yu, S. Yuan, L. Yang, Z. Liu, D. Yang, Effects of oxygen related thermal donors on the performance of silicon heterojunction solar cells. *Sol. Energy Mater. Sol. Cells* **179**, 17–21 (2018)
- H. Lu, D. Yang, L. Li, Z. Ye, D. Que, Thermal warpage of Czochralski silicon wafers grown under a nitrogen ambience. *Phys. Status Solidi A* **169**(2), 193–198 (1998)
- G. Mannino, V. Privitera, S. Scalesi, S. Libertino, E. Napolitani, P. Pichler, N.E. Cowern, Effect of oxygen on the diffusion of nitrogen implanted in silicon. *Electrochem. Solid-State Lett.* **7**(8), G161–G163 (2004)
- J. Murphy, A. Giannattasio, S. Senkader, R. Falster, P. Wilshaw, Nitrogen transport in float-zone and Czochralski silicon investigated by dislocation locking experiments. *Phys. Status Solidi A* **202**(5), 926–930 (2005)
- J.D. Murphy, C. Alpess, A. Giannattasio, S. Senkader, R. Falster, P. Wilshaw, Nitrogen in silicon: transport and mechanical properties. *Nucl. Instrum. Methods Phys. Res., Sect. B* **253**(1), 113–117 (2006)
- M. Nakatsu, A. Hashimoto, A. Natsume, N. Inoue, H. Ono, Measurement of nitrogen concentration in cz-si below 1014/cm³ by IR absorption spectroscopy, in *High Purity Silicon VIII: Proceedings of the International Symposium*, (The Electrochemical Society, 2004), p. 102
- J. Nelson, P. Schultz, A. Wright, Valence and atomic size dependent exchange barriers in vacancy-mediated dopant diffusion. *Appl. Phys. Lett.* **73**(2), 247–249 (1998)
- T. Nozaki, Y. Yatsurugi, N. Akiyama, Charged particle activation analysis for carbon, nitrogen and oxygen in semiconductor silicon. *J. Radioanal. Nucl. Chem.* **4**(1), 87–98 (1970)
- H. Ono, M. Horikawa, Quantitative detection of small amount of nitrogen in Czochralski-grown silicon crystals. *Jpn. J. Appl. Phys.* **42**(3B), L261 (2003)
- V. Orlov, H. Richter, A. Fischer, J. Reif, T. Müller, R. Wahlich, Mechanical properties of nitrogen-doped CZ silicon crystals. *Mater. Sci. Semicond. Process.* **5**(4–5), 403–407 (2002)
- P. Pavlov, E. Zorin, D. Tetelbaum, A. Khokhlov, Nitrogen as dopant in silicon and germanium. *Phys. Status Solidi A* **35**(1), 11–36 (1976)
- M. Porrini, M. Pretto, R. Scala, Measurement of nitrogen in Czochralski silicon by means of infrared spectroscopy. *Mater. Sci. Eng. B* **102**(1), 228–232 (2003)
- M. Qi, S. Tan, B. Zhu, P. Cai, W. Gu, X. Xu, T. Shi, D. Que, L. Li, The evidence for interaction of the N-N pair with oxygen in Czochralski silicon. *J. Appl. Phys.* **69**(6), 3775–3777 (1991)
- D. Que, X. Chen, *Silicon Materials Science and Technology* (Zhejiang University Press, Hangzhou, China, 2000). (in Chinese)
- D. Que, L. Li, Y. Lin, Nitrogen protective ambience for Czochralski growth of silicon. Chinese Patent CN85100295, 1985
- D. Que, L. Li, X. Chen, Nitrogen gas doping in Czochralski silicon. Chinese Patent CN87105811, 1987
- D. Que, L. Li, X. Chen, Y. Lin, J. Zhang, X. Zhou, J. Yang, Czochralski silicon crystal growth in nitrogen atmosphere under reduced pressure. *Sci. China Ser. A Math. Phys. Astron. Technol. Sci.* **34**(8), 1017–1024 (1991)

- C. Reimann, M. Trempa, J. Friedrich, G. Müller, About the formation and avoidance of C and N related precipitates during directional solidification of multi-crystalline silicon from contaminated feedstock. *J. Cryst. Growth* **312**(9), 1510–1516 (2010)
- S. Richter, J. Bauer, O. Breitenstein, Growth of carbon and nitrogen containing precipitates in crystalline solar silicon and their influence on solar cells. *Phys. Status Solidi RRL* **11**(2), 1600354 (2017)
- H. Sawada, H. Kawakami, First-principles calculation of the interaction between nitrogen atoms and vacancies in silicon. *Phys. Rev. B* **62**(3), 1851 (2000)
- H. Sawada, K. Kawakami, A. Ikari, W. Ohashi, Atomistic model of nitrogen-pair diffusion in silicon. *Phys. Rev. B* **65**(7), 075201 (2002)
- S. Schoenfelder, A. Bohne, J. Bagdahn, Comparison of test methods for strength characterization of thin solar wafer. in *Proceedings of 22nd European Photovoltaic Solar Energy Conference*, Milan, Italy, 2007, vol 7
- S. Schoenfelder, A. Sampson, V. Ganapati, R. Koepge, J. Bagdahn, T. Buonassisi, Quantitative stress measurements of bulk microdefects in multicrystalline silicon. 24th EUPVSEC:977–980 (2009)
- P.A. Schultz, J.S. Nelson, Fast through-bond diffusion of nitrogen in silicon. *Appl. Phys. Lett.* **78** (6), 736–738 (2001)
- L.L. Snead, T. Nozawa, Y. Katoh, T.-S. Byun, S. Kondo, D.A. Petti, Handbook of SiC properties for fuel performance modeling. *J. Nucl. Mater.* **371**(1–3), 329–377 (2007)
- A. Soiland, E. Øvrelid, T. Engh, O. Lohne, J. Tuset, Ø. Gjerstad, SiC and Si₃N₄ inclusions in multicrystalline silicon ingots. *Mater. Sci. Semicond. Process.* **7**(1), 39–43 (2004)
- N. Stoddard, P. Pichler, G. Duscher, W. Windl, Ab initio identification of the nitrogen diffusion mechanism in silicon. *Phys. Rev. Lett.* **95**(2), 025901 (2005)
- M. Suezawa, K. Sumino, H. Harada, T. Abe, Nitrogen-oxygen complexes as shallow donors in silicon crystals. *Jpn. J. Appl. Phys.* **25**(10A), L859 (1986)
- M. Suezawa, K. Sumino, H. Harada, T. Abe, The nature of nitrogen-oxygen complexes in silicon. *Jpn. J. Appl. Phys. Part 1* **27**(1), 62–67 (1988). <https://doi.org/10.1143/jjap.27.62>
- K. Sumino, I. Yonenaga, M. Imai, T. Abe, Effects of nitrogen on dislocation behavior and mechanical strength in silicon crystals. *J. Appl. Phys.* **54**(9), 5016–5020 (1983)
- Y. Tokumaru, H. Okushi, T. Masui, T. Abe, Deep levels associated with nitrogen in silicon. *Jpn. J. Appl. Phys.* **21**(7A), L443 (1982)
- M. Trempa, C. Reimann, J. Friedrich, G. Müller, The influence of growth rate on the formation and avoidance of C and N related precipitates during directional solidification of multi crystalline silicon. *J. Cryst. Growth* **312**(9), 1517–1524 (2010)
- L. Vandeperre, F. Giuliani, S. Lloyd, W. Clegg, The hardness of silicon and germanium. *Acta Mater.* **55**(18), 6307–6315 (2007)
- J. Vedde, P. Gravesen, The fracture strength of nitrogen doped silicon wafers. *Mater. Sci. Eng. B* **36** (1–3), 246–250 (1996)
- V.V. Voronkov, R.J. Falster, Nitrogen diffusion and interaction with oxygen in Si. in *Solid State Phenomena*, 2004. Trans Tech Publ, pp. 83–92
- P. Wagner, R. Oeder, W. Zulehner, Nitrogen-oxygen complexes in Czochralski-silicon. *Appl. Phys. A* **46**(2), 73–76 (1988)
- H. Wagner, H.C. Alt, W. von Ammon, F. Bittersberger, A. Huber, L. Koester, N-O related shallow donors in silicon: stoichiometry investigations. *Appl. Phys. Lett.* **91**(15), 152102 (2007)
- G. Wang, D. Yang, D. Li, Q. Shui, J. Yang, D. Que, Mechanical strength of nitrogen-doped silicon single crystal investigated by three-point bending method. *Phys. B Condens. Matter* **308**, 450–453 (2001)
- D. Yang, X. Yu, Nitrogen in Silicon. *Defect Diffus. Forum* **230–232**, 199–220 (2004)
- D. Yang, D. Que, K. Sumino, Nitrogen effects on thermal donor and shallow thermal donor in silicon. *J. Appl. Phys.* **77**(2), 943–944 (1995)
- D. Yang, R. Fan, L. Li, D. Que, K. Sumino, Effect of nitrogen–oxygen complex on electrical properties of Czochralski silicon. *Appl. Phys. Lett.* **68**(4), 487–489 (1996)

- D. Yang, X. Yu, D. Que, Nitrogen doping in casting multicrystalline silicon by melting feedstocks in nitrogen ambience. Chinese Patent CN101597790, 2009
- Y. Yatsurugi, N. Akiyama, Y. Endo, T. Nozaki, Concentration, solubility, and equilibrium distribution coefficient of nitrogen and oxygen in semiconductor silicon. *J. Electrochem. Soc.* **120**(7), 975–979 (1973)
- I. Yonenaga, Dislocation–impurity interaction in Si. *Mater. Sci. Eng. B* **124**, 293–296 (2005)
- I. Yonenaga, K. Sumino, K. Hoshi, Mechanical strength of silicon crystals as a function of the oxygen concentration. *J. Appl. Phys.* **56**(8), 2346–2350 (1984)
- I. Yonenaga, T. Taishi, X. Huang, K. Hoshikawa, Dislocation–impurity interaction in Czochralski-grown Si heavily doped with B and Ge. *J. Cryst. Growth* **275**(1–2), e501–e505 (2005)
- X. Yu, D. Yang, X. Ma, J. Yang, L. Li, D. Que, Grown-in defects in nitrogen-doped Czochralski silicon. *J. Appl. Phys.* **92**, 188–194 (2002)
- X. Yu, D. Yang, K. Hoshikawa, Investigation of nitrogen behaviors during Czochralski silicon crystal growth. *J. Cryst. Growth* **318**(1), 178–182 (2011)
- X. Yu, J. Chen, X. Ma, D. Yang, Impurity engineering of Czochralski silicon. *Mater. Sci. Eng. R. Rep.* **74**(1), 1–33 (2013)
- S. Yuan, D. Hu, X. Yu, F. Zhang, H. Luo, L. He, D. Yang, Controllable Nitrogen Doping in Multicrystalline Silicon by Casting Under Low Cost Ambient Nitrogen. *Silicon* 1–6 (2018)
- H. Zhang, M. Stavola, M. Seacrist, Nitrogen-containing point defects in multi-crystalline Si solar-cell materials. *J. Appl. Phys.* **114**(9), 093707 (2013)